IEEE Access
Multidisciplinary ⋮ Rapid Review ⋮ Open Access Journal

Received 31 December 2023, accepted 8 January 2024, date of publication 16 January 2024,
date of current version 25 January 2024.

Digital Object Identifier 10.1109/ACCESS.2024.3354847

RESEARCH ARTICLE

Output Feedback Fault Tolerant Control for Linear Parameter Varying Plants Considering Imperfect Fault Information

OMAR AZEEM[1], MIRZA TARIQ HAMAYUN[1], SALMAN IJAZ[2,3], AND KHANSA TARIQ[4], (Graduate Student Member, IEEE)

[1]Department of Electrical and Computer Engineering, COMSATS University Islamabad, Lahore Campus, Lahore 54000, Pakistan
[2]Key Laboratory of More Electric Aircraft of Zhejiang Province, University of Nottingham, Ningbo 315100, China
[3]Control System Laboratory, University of Nottingham, Ningbo 315100, China
[4]Department of Electrical Engineering, Lahore University of Management Sciences (LUMS), Lahore 54792, Pakistan

Corresponding author: Salman Ijaz (salman.ijaz@nottingham.edu.cn)

This work is supported by the Natural Science Foundation of China with Project 62250410367.

ABSTRACT This study focuses on the design of an integral sliding mode-based fault-tolerant control allocation (ISM-FTCA) scheme for the class of uncertain linear parameter varying (LPV) systems. The objective is to tackle the fault occurring in the actuator channel by exploiting available redundancy through a control allocation (CA) scheme in an output feedback framework. In this work, the assumption on the estimation of actuator effectiveness level, which was previously considered (in the existing literature) to be perfect coming from fault diagnosis and identification (FDI) scheme, is relaxed due to its bit conservatism nature. The uncertain system dynamics, originating due to faults, failures, and imperfect fault information, are catered to by designing a virtual control law using the LPV output ISM control strategy. An unknown input LPV observer is designed to provide the estimate of unmeasured plant states to the virtual control law. This work thoroughly investigates the closed-loop dynamics of the uncertain LPV system, utilizing the small gain theorem to develop criteria for stability. These conditions provide crucial insights into the performance and robustness of the suggested strategy. Finally, the efficiency of the proposed control scheme is verified in the simulation environment by using a nonlinear 6-degree-of-freedom dynamic model of the octarotor unmanned aerial vehicle (UAV) system. Numerical simulations under different faults and failures conditions and in the presence of imprecise estimation validate the closed-loop performance close to nominal scenarios.

INDEX TERMS Fault tolerance, sliding mode control, robust control, aerospace control, control system synthesis.

I. INTRODUCTION

Safety is essential in aerospace systems. Despite being the safest mode of transportation, air travel is still susceptible to sudden actuator failure, sensor malfunctions, and even structural damage [1]. These damages and faults can result in non-equilibrium flight conditions together with varied inertial and aerodynamic properties, additional sources of uncertainty, and even reduced flight authority. Therefore, it is crucial to study fault-tolerant control (FTC), which automatically accommodates errors and uncertainties while maintaining stability and ideal performance.

Linear parameter varying (LPV) has gained significant interest in recent decades due to its applicability in systems with real-time sensor input-output data. This approach allows the tuning of controller parameters in the presence of parameter variations [2], [3]. LPV control method was initially introduced in the work of [4] to the author's best knowledge.

The associate editor coordinating the review of this manuscript and approving it for publication was Haibin Sun.

Now, LPV paradigm has become the standard formulation in the field of systems and control, serving as the established formulation for tasks such as model identification, analysis, and controller synthesis. Within the field of FTC for LPV systems, numerous noteworthy findings are documented in the current literature. Such as in [5], the actuator fault-tolerant control was achieved by placing the virtual actuator between the faulty plant and the nominal system. The authors in [6] proposed an adaptive polytopic observer-based state feedback control law to deal with the time-varying actuator faults in the LPV system. A reconfigurable PID fault-tolerant tracking control law was developed in [7] for the LPV systems influenced by actuator faults and external disturbance. An event-triggered mechanism-based FTC approach was proposed for the LPV system in [8] where the fault observer is used to estimate the fault.

In recent years, there has been a notable advancement in the development of Linear Parameter-Varying (LPV) synthesis methodologies for applications in aerospace, particularly fault-tolerant systems and fault diagnosis. The adoption of LPV frameworks in this context is attributed to their capability to ensure stability and resilience across a broad spectrum of airborne scenarios. The authors in [9] developed a time-driven switching controller for a switched LPV system that incorporates actuator faults. This controller was successfully implemented to aero engines. LPV control technique was also utilized in [10] to perform the aggressive maneuvering of unmanned helicopter system where actuator fault and system states are estimated using an unknown input observer (UIO). In [11], a robust active FTC scheme is proposed for a polytopic LPV system and is applied to a vertical take-off landing (VTOL) aircraft system. The LPV controller is based on sliding-mode-based state feedback control equipped with H_∞ performance criteria. Addressing the issue of effective utilization of actuator redundancy in aircraft dissimilar redundant actuation system, [12] presented an adaptive LPV integral SMC-based control approach. This controller is tailored to mitigate the effect of actuator faults. However, the complete failure cannot be handled by the proposed scheme which presents a more severe challenge. Recently in [13], a robust estimated based dual mode predictive FTC scheme is proposed for LPV system to deal with actuator fault while also taking into account limits on the system's states and input. For the class of switched LPV system, the authors in [2] proposed an active FTC approach where both input and output matrices can vary with parameters. Through a unique Lyapunov function approach, dependent on both dwell time and parameter variations, an integrated scheme is designed to address fault detection, estimation, and compensation simultaneously. Fault estimation plays a crucial role in active FTC by providing the ability to detect, isolate, and estimate faults in real time. Some recent works on fault estimation schemes hold valuable results in the simultaneous estimation of systems states, faults, and disturbances for the class of nonlinear and T-S fuzzy systems, such as recently proposed in [14], [15], and [16]. In contrast, the proposed LPV-based UIO approach that is proposed in this paper can explicitly account for parameter variations, which makes it appropriate for systems with known parameter variations such as airplanes and UAVs.

The utilization of actuator redundancy is enhanced by the implementation of a control allocation (CA) scheme, which has been widely recognized as a successful strategy. This approach is particularly advantageous due to its ability to provide a flexible modular design [17]. One notable benefit of the CA scheme is its ability to allow for the independent design of the controller, without necessitating prior knowledge of the specific characteristics of the fault. The CA strategy is in charge of allocating control effort to the available healthy actuators whenever the specific actuator is prone to fault and failure. There are several elegant algorithms described for the CA approach such as pseudo-inverse scheme [18], daisy-chaining [19], convex optimization approach [20], and singular value decomposition approach [21]. Several notable results on the CA-based FTC scheme have been presented in recent years that deal with the class of linear-time invariant (LTI) systems such as see [22], [23], [24], [25], and [26]. In the context of the LPV system, several CA schemes have been proposed recently. One notable example is the dynamics CA scheme introduced by [27] in their work on the quadrotor system. In [28], an interval sliding mode observer-based online CA scheme is proposed for a non-minimum phase LPV system. In the output feedback framework, the authors in [29] presented an integral SMC-based CA scheme for over-actuated LPV systems to deal with actuator faults and failures. In this formulation, the virtual control law, derived from the ISMC approach, is transformed into physical control input through a fixed CA scheme. Likewise, SMC-based CA is proposed for the LPV system in [30] and is tested on a full-scale aircraft system, showcasing the maintenance of flight paths despite aileron and rudder faults. Recently in [31], the LPV SMC-based CA scheme is also applied to an octoplane UAV system that utilized the pseudo-inverse-based CA method to reconfigure control law. Compared to the extensively studied SMC-based CA scheme for the LTI scheme, less literature is available for the LPV system, particularly in the output feedback framework. In practice, the output feedback control is more appealing to the scientific community because, in reality, the whole states are rarely available at the output. In the existing work on output ISMC-based CA scheme, such as in [29], a fixed CA unit was used that only tolerates limited faults and failure combinations. In another work [30], the online CA scheme was proposed but the fault and failure information was assumed to be perfect which is not a practical assumption. Therefore, it is important to study the LPV-based FTC scheme that can deal with the faulty actuators by considering imperfect fault information (which is a realistic approach) obtained from the fault estimation module while actively reconfiguring the control signals amongst the redundant actuators. Moreover, it is also crucial to study the output feedback control which is more practical compared to full-state feedback.

Therefore, the goal of this research is to develop an output feedback FTC-based CA method for LPV systems that can cope with actuator faults and failures while maintaining nominal closed-loop performance and providing additional robustness towards the parameter variation. To cope with potential actuator faults and failures, an online CA scheme is presented first by performing the partitioning of the input distribution matrix that redistributes the virtual input signals amongst the available set of redundant actuators. The unknown system states are then estimated by using an LPV-based UIO unit which is known to be inherently robust to uncertainties making it well-suited for systems with unknown or time-varying parameters. Based on the estimated state information, a virtual LPV control law is designed using the output integral SMC technique. A detailed closed-loop stability (CLS) analysis is performed to prove the system stability under uncertainty that arises in the system due to faults, failures, and fault estimation errors. An LMI synthesis procedure is adopted to obtain the controller and observer gains. Finally, the proposed scheme is implemented on a nonlinear model of an octorotor UAV system. Nonlinear simulations under different faults and failure conditions are performed to demonstrate the effectiveness of the proposed scheme. Compared to the existing methods [21], [23], [29], [30], [32], [33], [34], the unique contribution and advantages of the proposed scheme are outlined as follows:

- In contrast to established ISMC-based online CA techniques tailored for linear time-invariant (LTI) systems [21], [23], [30], [32], [33], this work considered LPV system to formulate FTC law in the output feedback framework. A distinctive feature of this work involves a pioneering consideration of imperfections inherent in fault estimation units during FTC analysis. Unlike prior effort [29], [30], the current study meticulously accounts for challenges posed by imperfect estimations, thereby enhancing the robustness of the proposed method.
- Unlike existing studies in [29] and [34], the online CA unit can tolerate more combinations of faults and failures occurring in the actuator channel.
- The effectiveness of the enhanced system is thoroughly demonstrated through a two-step validation procedure. The initial validation process involves the utilization of LPV model of an octarotor UAV system. The adaptability of the suggested approach is further emphasized by its application to the six-degree-of-freedom nonlinear model of the octarotor UAV by using a two-loop control structure, thereby confirming its promise in other intricate systems.

II. PROBLEM FORMULATION

Consider an uncertain LPV system with faults and failures in the actuators and external disturbance, expressed as

$$\begin{aligned} \dot{x}_k(t) &= A_k(\rho_k)x_k(t) + B_k(\rho_k)W_k(t)u_k(t) + D_k(\rho_k)d_k(t,x_k) \\ y_k(t) &= C_k x_k(t), \end{aligned} \tag{1}$$

where $A_k(\rho_k) \in R^{n\times n}$, $B_k(\rho_k) \in R^{n\times m}$ and $D_k(\rho_k) \in R^{n\times q}$ represent system matrix, input distribution matrix, and disturbance matrix depend on the scheduling parameter ρ_k, whereas $C_k \in R^{p\times n}$ constitutes of an output matrix, $d_k(t,x_k)$ represents an external disturbance input matrix and $W_k(t) \in R^{m\times m}$ stands for a semi-positive definite diagonal effectiveness matrix defined as $W_k(t) = diag(w_1(t),..,w_m(t))$ where the time-varying diagonal entries $w_i(t)$ model the effectiveness level of the actuators and satisfy $0 \le w_i(t) \le 1$. For example, $w_i = 1$ implies that the relevant actuator is fault-free, and $0 < w_i(t) < 1$ denotes that the relevant actuator is working at a decreased efficiency owing to some amount of fault, while $w_i = 0$ denotes that the actuator has completely failed. In LPV plant (1), $\rho_k(t)$ belongs to a known bounded set i.e. $\Omega \subset R^r$ and matrices $A_k(\rho_k)$ and $B_k(\rho_k)$ dependent affinely on parameter vector ρ_k expressed as

$$X_k(\rho_k) = X_0 + \sum_{i=1}^{r} \rho_k X_k, \tag{2}$$

where $X_k(\rho_k) \in \{A_k(\rho_k), B_k(\rho_k)\}$. The fault considered in this work is treated as a multiplicative actuator fault. However, it can also affect the actuator channel in an additive way by defining $W_k(t) := 1 - K(t)$ such as see the earlier work [26], [35]. A layout of the overall control strategy is shown in Fig. 1. To resolve actuator redundancy, the parameter-dependent matrix $B_k(\rho_k)$ is first expressed as

$$B_k(\rho_k) = B_f E_k(\rho_k), \tag{3}$$

where $B_f \in R^{n\times m}$ is a fixed matrix and $E_k(\rho_k) \in R^{m\times m}$ is parameter dependent matrix depends on scheduling variable $\rho_k(t)$. In (3), the matrix B_f is further partitioned as

$$B_f = [B_1^T \quad B_2^T]^T, \tag{4}$$

where $B_1 \in R^{(n-l)\times m}$, $B_2 \in R^{l\times m}$ and $l < m$. The partitioning of B_f in (4) ensures $\|B_2\| \gg \|B_1\|$ which means that the components associated with B_2 have dominant contribution in delivering control effort compared to B_1. In the field of the aircraft system, the channel B_2 is often correlated with the equation of angular acceleration governing roll, pitch, and yaw dynamics because most of the control objectives can be attained by controlling the desired moments. By hypothesis, $\|B_1\|$ is assumed to be small. To create this separation, the permutation of states must usually be undertaken.

Remark: Note that the structure and formal representation of the LPV system in (1) is quite similar to the T-S fuzzy system. However, they differ in their underlying representation and methodology. LPV system focuses on linear variations in a deterministic manner, while the T-S fuzzy models use fuzzy logic to approximate nonlinear systems with a set of local linear models.

Assumption 1: From the partitioning of B_f in (4), it is assumed that the states can be scaled to ensure $B_2 B_2{}^T = I_l$ and $\|B_2\| = 1$.

Since $rank(B_2) = I_l$, therefore assumption 1 can be achieved without loss of generality. Considering (3) and (4),

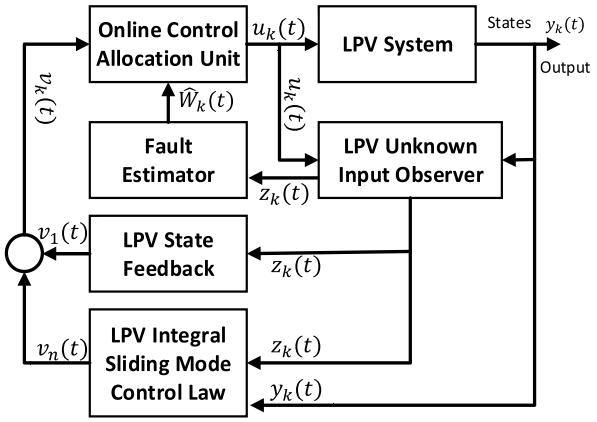

FIGURE 1. Layout of the proposed control strategy.

the LPV uncertain system in (1) can be written as

$$\dot{x}_k(t) = A_k(\rho_k)x_k(t) + \begin{bmatrix} B_1E_k(\rho_k)W_k(t) \\ B_2E_k(\rho_k)W_k(t) \end{bmatrix} u_k(t) + D_k(\rho_k)d_k(t, x_k). \tag{5}$$

Assumption 2: The information of actuator healthiness level $W_k(t)$ provided by the FDI unit is not perfect.

To model the level of imperfection in estimated fault information, we define

$$W_k(t) = (I_m - \Delta_k(t))\widehat{W}_k(t), \tag{6}$$

where $\widehat{W}_k(t) = \text{diag}\{\hat{w}_1(t), \ldots, \hat{w}_m(t)\}$ is the estimation of actuator effectiveness and the scalars $\hat{w}_i(t), i = 1 \ldots m$ are assumed to satisfy $0 \leq \hat{w}_i(t) \leq 1$. In (6), $\Delta_k(t) = diag\{\delta_1(t), \ldots, \delta_m(t)\}$ denotes the error in estimation and $\delta_m(t)$ represents the imperfection level in fault estimation. The uncertain system dynamics (5) after considering the effect of imperfection (6) is obtained as

$$\dot{x}_k(t) = A_k(\rho_k)x_k(t) + \begin{bmatrix} B_1E_k(\rho_k)(1 - \Delta_k(t))\widehat{W}_k(t) \\ B_2E_k(\rho_k)(1 - \Delta_k(t))\widehat{W}_k(t) \end{bmatrix} u_k(t) + D_k(\rho_k)d_k(t, x_k). \tag{7}$$

Remark: In the earlier work on the FTC of LPV system [29], the fault information was assumed to be perfectly available. Nevertheless, this study incorporates a fault estimation error $\delta_k(t)$ when measuring the efficacy of each actuator (6). To maintain the estimate within the theoretical bounds, a saturation block with a limit [0 1] is used before the information sent to the CA unit. In the next section, a comprehensive closed-loop stability analysis will be conducted taking into account imperfection in fault estimation. The objective is to assess the maximum estimation error that the suggested method can tolerate.

III. VIRTUAL CONTROL LAW DESIGN

This subsection introduces a virtual control law $v_k(t) \in R^l$ which is defined as the total amount of control effort generated by the actuators

$$v_k(t) = B_2E_k(\rho_k)u_k(t). \tag{8}$$

The choice of physical control law in (8) is considered as

$$u_k(t) = E_k^{\dagger}(\rho_k)\, v_k(t), \tag{9}$$

where

$$E_k^{\dagger}(\rho_k) = \widehat{W}_k(t)(E_k(\rho_k))^{-1}B_2^T(B_2(E_k(\rho_k))\widehat{W}_k(t) \times (E_k(\rho_k))^{-1}B_2^T)^{-1}, \tag{10}$$

is one of the choice of a weighted right pseudo inverse of $B_2(E_k(\rho_k))$. Using (9), the expression in (7), with respect to virtual control $v_k(t)$, can be expressed as

$$\dot{x}_k(t) = A_k(\rho_k)x_k(t) + \begin{bmatrix} B_1E_k(\rho_k)(1 - \Delta_k(t))\widehat{W}_kE_k^{\dagger}(\rho_k) \\ B_2E_k(\rho_k)(1 - \Delta_k(t))\widehat{W}_kE_k^{\dagger}(\rho_k) \end{bmatrix} \times v_k(t) + D_k(\rho_k)d_k(t, x_k). \tag{11}$$

With the choice of

$$\hat{v}_k(t) = B_2E_k(\rho_k)\widehat{W}_k(E_k(\rho_k))\dagger v_k(t), \tag{12}$$

the expression in (11) is further written for convenience as

$$\dot{x}_k(t) = A_k(\rho_k)x_k(t) + \underbrace{\begin{bmatrix} B_1E_k(\rho_k)(1 - \Delta_k(t))E_k^{\ddagger}(\rho_k) \\ B_2E_k(\rho_k)(1 - \Delta_k(t))E_k^{\ddagger}(\rho_k) \end{bmatrix}}_{B_w(\rho_k)} \hat{v}_k(t) + D_k(\rho_k)d_k(t, x_k), \tag{13}$$

where

$$E_k^{\ddagger}(\rho_k) = \widehat{W}_k^2(t)(E_k(\rho_k))^{-1}B_2^T(B_2(E_k(\rho_k))\widehat{W}_k^2(t) \times (E_k(\rho_k))^{-1}B_2^T)^{-1} \tag{14}$$

is also a weighted right pseudo inverse of $B_2E_k(\rho_k)$, provided that $\det(B_2(E_k(\rho_k))\widehat{W}_k^2(E_k(\rho_k))^{-1}B_2{}^T \neq 0$.

A. NOMINAL LPV CONTROLLER

The nominal virtual control law to be formed is based on the fault-free system, thus taking into account the case when the actuator efficiency estimate is ideal i.e. $\Delta_k(t) = 0$ and system does not have actuator faults,i.e $\widehat{W}_k(t) = I_m$, then the uncertain system in (13) can be simplified as

$$\dot{x}_k(t) = A_k(\rho_k)x_k(t) + \underbrace{\begin{bmatrix} B_1B_2^T \\ B_2B_2^T \end{bmatrix}}_{B_v} v_k(t), \tag{15}$$

where $B_v = B_fB_2^T$. Assume a positive definite matrix $P \in R^{n\times n}$ and a feedback gain $F(\rho_k) \in R^{l\times n}$ exists such that

$$\big(A_k(\rho_k) - B_vF(\rho_k)\big)^T P + P\big(A_k(\rho_k) - B_vF(\rho_k)\big) < 0, \tag{16}$$

then

$$\dot{x}_k(t) = \big(A_k(\rho_k) - B_vF(\rho_k)\big)x_k(t) \tag{17}$$

is quadratically stable. The feedback gain $F(\rho_k)$ is formulated to minimize the linear quadratic regulator (LQR) cost function $\int(x_kQ_k^Tx_k + u_kR_ku_k)dt$ where Q_k and R_k represent symmetric-positive-definite (s.p.d.) matrices. The specific method of selecting $F(\rho_k)$ is derived from the work of [36] and is not discussed in this paper.

B. SWITCHING FUNCTION DESIGN

The nominal control law ensures stability in fault-free condition. However, the uncertainty arose due to system faults and failures can influence the system dynamics. In this subsection, a nonlinear LPV ISMC law that interfaces with the nominal control law is designed to enhance the robustness. The first step is to define a switching surface $S = \{x_k \in R^n : \sigma_k(t) = 0\}$, where $\sigma_k(t)$ denotes the switching function defined as

$$\sigma_k(t) := G_k y_k(t) - G_k y_k(0) + \int_0^t F(\rho_k)\hat{x}_k(\tau)d\tau, \quad (18)$$

where $G_k \in R^{l\times n}$ is the design choice. In this paper, the matrix G_k in (18) is selected as

$$G_k := B_2((C_kB_f)^T C_kB_f)^{-1}(C_kB_f)^T. \quad (19)$$

The choice of G_k in (18) assures that $G_kC_kB_v = I_l$, which is useful in deriving the expression of virtual control law.

Assumption 3: In this paper, we considered $rank(B_f) = rank(C_kB_f) = m$.

The relevant control expression and the stability of the sliding dynamics are derived by taking switching function (18) derivative which yields

$$\dot{\sigma}_k(t) = F(\rho_k)\hat{x}_k(t) + G_k\dot{y}_k(t). \quad (20)$$

By substituting (1) and (13), the switching function derivative (20) can be expressed as

$$\begin{aligned}\dot{\sigma}_k(t) &= G_kC_k\dot{x}_k(t) + F(\rho_k)\hat{x}_k(t)\\ &= G_kC_kA_k(\rho_k)x_k(t) + G_kC_kB_w(\rho_k)\hat{v}_k(t)\\ &\quad + G_kC_kD_k(\rho_k)d_k(t,x_k) + F(\rho_k)\hat{x}_k(t). \end{aligned} \quad (21)$$

Assume that during sliding $\sigma_k(t) = \dot{\sigma}_k(t) = 0$, therefore, the equivalent control representation can be written as [37],

$$\begin{aligned}\hat{v}_{eq}(t) = -(G_kC_kB_w(\rho_k))^{-1}\big(&F(\rho_k)\hat{x}_k(t)\\ &+ G_kC_kA_k(\rho_k)x_k(t) + G_kC_kD_k(\rho_k)d_k(t,x_k)\big).\end{aligned} \quad (22)$$

With the choice of G_k in (19), the following simplification is made as

$$G_kC_kB_w(\rho_k) = I - B_2\psi(t,\rho_k), \quad (23)$$

where

$$\psi(t,\rho_k) = E_k(\rho_k)\Delta_k(t)E_k^{\ddagger}(\rho_k). \quad (24)$$

Substitute (23) into (22), we get,

$$\begin{aligned}\hat{v}_{eq}(t) = -(I - B_2\psi(t,\rho_k))^{-1}&(F(\rho_k)\hat{x}_k(t)\\ &+ G_kC_kA_k(\rho_k)x_k(t) + G_kC_kD_k(\rho_k)d_k(t,x_k)).\end{aligned} \quad (25)$$

Next, the dynamics associated with the sliding surface is obtained by substituting the equivalent virtual control law (25) into (13) which yields

$$\begin{aligned}\dot{x}_k(t) = A_k(\rho_k)x_k(t) - B_m((F(\rho_k)\hat{x}_k(t) + G_kC_kA_k(\rho_k)\\ \times x_k(t)) + (1 - B_\omega(\rho_k)(G_kC_kB_\omega(\rho_k))D_k(\rho_k)d_k(t,x_k),\end{aligned} \quad (26)$$

where

$$B_m := \left[B_1E_k(\rho_k)(1-\Delta_k(t))E_k^{\ddagger}(\rho_k)(I - B_2\psi(t,\rho_k))^{-1}I_l\right]. \quad (27)$$

Remark: With the choice of G_k in (19) and utilizing the results of proposition 3 in [37], we can conclude that the Euclid norm of uncertain term is equal to one *i.e.*$\|\Lambda^*\| = 1$. Therefore, $\|\Lambda^*D_k(\rho_k)d_k(t,x_k)\| \le \|D_k(\rho_k)d_k(t,x_k)\|$.

Next, add and subtract the term $B_v(F(\rho_k)\hat{x}_k(t) + G_kC_kA_k(\rho_k)x_k(t))$ to the right hand side and using $e_k(t) = x_k(t) - \hat{x}_k(t)$, the system (26) can be additionally written in a form suitable for stability analysis

$$\begin{aligned}\dot{x}_k(t) = (-B_vG_kC_kA_k(\rho_k) + A_k(\rho_k) - B_vF(\rho_k))x_k(t)\\ + B_vF(\rho_k)e_k(t) + \tilde{B}\tilde{\Phi}(t)(F(\rho_k)(x_k(t) - e_k(t))\\ + G_kC_kA_k(\rho_k)x_k(t)) + D_k(\rho_k)d_k(t,x_k),\end{aligned} \quad (28)$$

where

$$\tilde{B} := \begin{bmatrix} I_{n-l} \\ 0 \end{bmatrix} \quad (29)$$

and $\tilde{\Phi}(t)$ denotes the system uncertainty which is defined as

$$\begin{aligned}\tilde{\Phi}(t) = B_1B_2^T - B_1E_k(\rho_k)(I - \Delta_k(t))E_k^{\ddagger}(\rho_k)\\ \times (I - B_2\psi(t,\rho_k))^{-1}.\end{aligned} \quad (30)$$

Let's define an allowable a set of actuator faults that can be tolerated as

$$\begin{aligned}W_\delta = \{(w_1,\ldots,w_m) \in I_\delta : (G_kC_kB_w(\rho_k))^T\\ \times (G_kC_kB_w(\rho_k)) > \epsilon I\},\end{aligned} \quad (31)$$

where $I_\delta = [0 \quad 1] \times \ldots \times [0 \quad 1]$ and $0 < \epsilon \le 1$. It is necessary to note that when estimation of actuator effectiveness is perfect *i.e.*$\Delta_k(t) = 0$ and all actuators are working perfectly i.e $\widehat{W}_k(t) = I$ and $d_k(t,x_k) = 0$, the term $\psi(t,\rho_k) = 0$ in (6), therefore the matrix $(G_kC_kB_w(\rho_k))^T(G_kC_kB_w(\rho_k)) = I$ and hence the set $W_\delta \neq \emptyset$. It can be easily shown that

$$\begin{aligned}\left\|(G_kC_kB_w)^{-1}\right\| &= \left\|(I - B_2\psi(t,\rho_k))^{-1}\right\|\\ &= (I - \|B_2\psi(t,\rho_k)\|)^{-1}\\ &< \frac{1}{1 - \frac{\Delta_{max}c_o}{\sqrt{\epsilon}}},\end{aligned} \quad (32)$$

where $c_o = max_{\rho\in\Omega}\|E_k(\rho_k)\|\left\|E_k(\rho_k)^{-1}\right\|$ and $\Delta_{max} = \|\Delta_k(t)\|$. The bounded condition in (32) is an important condition, where $\frac{\Delta_{max}c_o}{\sqrt{\epsilon}} < 1$ and will be incorporated in the analysis of CLS.

IV. LPV OBSERVER DESIGN

In this paper, we assumed only the measured outputs $y_k(t)$ to be accessible. However, the design of virtual control law requires the information of system states. To reconstruct all the state vector, a full order observer can be developed in this scenario. Considering the imperfect fault estimation (6) given by the FDI scheme, the uncertain LPV system in (1) can alternatively be expressed as

$$\dot{x}_k(t) = A_k(\rho_k)x_k(t) + B_k(\rho_k)(I - \hat{K})u_k(t) - B_k(\rho_k) \times \Delta_k(t)(I - \hat{K})u_k(t) + D_k(\rho_k)d_k(t, x_k), \quad (33)$$

where $\hat{K} := I - \widehat{W}_k$. The matrix $\hat{K} := diag[\hat{k}_1, \ldots, \hat{k}_m]$ and the diagonal elements k_i satisfy $0 \leq \hat{k}_m \leq 1$. In uncertain LPV plant given in (33), $\hat{K}u_k(t)$ is regarded as an unknown input. The suggested LPV observer's structure is as follows:

$$\dot{z}_k(t) = M(\rho_k)z_k(t) + T(\rho_k)B_k(\rho_k)u_k(t) + L(\rho_k)y_k(t) \quad (34)$$

$$\hat{x}_k(t) = z_k(t) + H(\rho_k)y_k(t), \quad (35)$$

where the matrices $M(\rho_k) \in R^{n\times n}, T(\rho_k) \in R^{n\times n}, H(\rho_k) \in R^{n\times p}$ are selected such that the unknown input term $\hat{K}u_k(t)$ can be decoupled from the error dynamics. In (34), $\hat{x}_k(t)$ represents the estimated state. Next define $e_k(t) = x_k(t) - \hat{x}_k(t)$, and time derivative of $e_k(t)$ after substituting (33) and (34) is written as

$$\begin{aligned}
&\dot{e}_k(t)\\
&= (A_k(\rho_k)x_k(t) + B_k(\rho_k)(I - \hat{K})u_k(t) - B_k(\rho_k)\Delta_k(t)\\
&\quad \times (I - \hat{K})u_k(t) + D_k(\rho_k)d_k(t, x_k) - M(\rho_k)z_k(t) - T(\rho_k)\\
&\quad \times B(\rho_k)u_k(t) - L(\rho_k)y_k(t) - H(\rho_k)\dot{y}_k(t) - \dot{H}(\rho_k)y_k(t)\\
&= (I_n - H(\rho_k)C_k)A_k(\rho_k)x_k(t) + (I_n - H(\rho_k)C_k)B(\rho_k)u_k(t)\\
&\quad - (I_n - H(\rho_k)C_k)B_k(\rho_k)\hat{K}u_k(t) - (I_n - H(\rho_k)C_k)B_k(\rho_k)\\
&\quad \times \Delta_k(t)u_k(t) + (I_n - H(\rho_k)C_k)B_k(\rho_k)\Delta_k(t)\hat{K}u_k(t)\\
&\quad - M(\rho_k)z_k(t) + (I_n - H(\rho_k)C_k)D_k(\rho_k)d_k(t, x_k). \quad (36)
\end{aligned}$$

With the appropriate choice of design matrices $H(\rho_k)$ and $T(\rho_k)$ in (36), in particular,

$$\begin{aligned}
H(\rho_k) &= B_k(\rho_k)((C_kB_k(\rho_k))^T C_kB_k(\rho_k))^{-1}((C_kB_k(\rho_k))^T\\
T(\rho_k) &= I_n - H(\rho_k)C_k \quad (37)
\end{aligned}$$

and by selecting $L(\rho_k) = L_1(\rho_k) + L_2(\rho_k)$, the unknown input term $B_k\hat{K}u_k(t)$ is separated from the system error dynamics (36), yielding

$$\begin{aligned}
\dot{e}_k(t) &= T(\rho_k)(A_k(\rho_k)x_k(t) - M(\rho_k)(\hat{x}_k(t)\\
&\quad - H(\rho_k)y_k(t)) - L_1(\rho_k)y_k(t) - L_2(\rho_k)y_k(t)\\
&\quad + T(\rho_k)D_k(\rho)d_k(t, x_k) - \dot{H}(\rho_k)y_k(t), \quad (38)
\end{aligned}$$

where, $rank(C_kB_k(\rho_k)) = rank(B_k(\rho_k)) = m$ and the choice of $H(\rho_k)$ and $T(\rho_k)$ in (37) ensures that $T(\rho_k)B_k(\rho_k) = 0$.

Assumption 4: Assume that the pair $(T(\rho_k)A_k(\rho_k), C_k)$ is detectible for all $\rho_k \in \Omega$.

Using the appropriate design of $L_2(\rho_k)$ and $M(\rho_k)$ specifically,

$$\begin{aligned}
L_2(\rho_k) &= M(\rho_k)H(\rho_k)\\
M(\rho_k) &= T(\rho_k)A_k(\rho_k) - L_1(\rho_k)C_k, \quad (39)
\end{aligned}$$

the error dynamics in (36) is written as

$$\begin{aligned}
\dot{e}_k(t) &= (T(\rho_k)A_k(\rho_k) - L_1(\rho_k)C_k)x_k(t) - M(\rho_k)x_k(t)\\
&\quad + M(\rho_k)e_k(t) - \dot{H}(\rho_k)C_kx_k(t) + T(\rho_k)D_k(\rho_k)d_k(t, x_k) \quad (40)
\end{aligned}$$

and further simplification leads to the form

$$\dot{e}_k(t) = M(\rho_k)e_k(t) - \dot{H}(\rho_k)C_kx_k(t) + T(\rho_k)D_k(\rho_k)d_k(t, x_k). \quad (41)$$

Assumption 5: The disturbance/uncertainty function $d_k(t, x_k)$ satisfies the following equality $d_k(t, x_k) = \psi_k(t, x_k)x_k(t)$ where $\|\psi_k(t, x_k)\| \leq \bar{\psi}_k$ and $\bar{\psi}_k$ denotes the bound on uncertainty term which is assumed to be known.

Now consider a candidate function $V_o(t) = e_k^T P_o e_k$, where P_o is defined as positive definite symmetric matrix derived from the solution $P_oM(\rho_k) + M^T(\rho_k)P_o = -I$ for all $\rho_k \in \Omega$.

Then the time derivative of $V_o(t)$ gives

$$\dot{V}_o(t) = \dot{e}_k^T P_o e_k + e_k^T P_o \dot{e}_k. \quad (42)$$

Substitute (41) into (42), we get

$$\begin{aligned}
&\dot{V}_o(t)\\
&= e_k(P_oM(\rho_k) + M^T(\rho_k)P_o)e_k^T - 2e_k^T P_o\dot{H}(\rho_k)\\
&\quad \times C_k\hat{x}_k(t) + 2e_k^T P_oT(\rho_k)D_k(\rho_k)d_k(t, x_k)\\
&\leq -\|e_k\|^2 - 2\|e_k\|\|P_o\|\left\|\dot{H}(\rho_k)C_k\right\|\left\|\hat{x}_k(t)\right\| + 2\|e_k(t)\|\\
&\quad \times \|P_o\|\|T(\rho_k)\|\|D_k(\rho_k)\|\|\psi_k(t, x_k)\|\|x_k(t)\|)\\
&\leq -\|e_k\|^2 - 2\|e_k\|\|P_o\|(\left\|\dot{H}(\rho_k)C_k\right\| - \|T(\rho_k)\|\|D_k(\rho_k)\\
&\quad \times \|\psi_k(t, x_k)\|)\|x_k(t)\|. \quad (43)
\end{aligned}$$

Hence, an appropriate choice of $L_1(\rho_k)$ yields convergence of error dynamics asymptotically.

A. ANALYSIS OF CLOSED-LOOP SYSTEM STABILITY

Prior to CLS analysis, an augmented system is created by combining the LPV uncertain system (28) and observer error system (41) as

$$\begin{bmatrix}\dot{e}_k(t)\\ \dot{x}_k(t)\end{bmatrix} = A_a(\rho_k)\begin{bmatrix}e_k(t)\\ x_k(t)\end{bmatrix} + B_a\Lambda(t)C_a(\rho_k)\begin{bmatrix}e_k(t)\\ x_k(t)\end{bmatrix}, \quad (44)$$

where

$$\begin{aligned}
A_a(\rho_k) &= \begin{bmatrix}M(\rho_k) & 0\\ B_vF(\rho_k) & A_c(\rho_k) - B_vF(\rho_k)\end{bmatrix}\\
A_c(\rho_k) &= (I - B_vG_kC_k)A_k(\rho_k)\\
B_a(\rho_k) &= \begin{bmatrix}-\dot{H}(\rho_k)C_k + (1 - H(\rho_k)C_k)D_k(\rho_k)\bar{\psi}_k & 0 & 0\\ 0 & \tilde{B} & \tilde{B}\end{bmatrix}, \quad (45)
\end{aligned}$$

and

$$C_a(\rho_k) = \begin{bmatrix} 0 & I \\ -F(\rho_k) & G_k C_k A_k(\rho_k) + F(\rho_k) \\ 0 & I \end{bmatrix}, \quad (46)$$

and $\Lambda(t)$ in (44) is an uncertain term defined as

$$\Lambda(t) = diag(0, \tilde{\Phi}(t), 0). \quad (47)$$

For the analysis of the stability of closed-loop system, it is appropriate to examine augmented system (44) in $(e_k, \hat{x}_k)$ coordinates system, therefore by utilizing $e_k(t) = x_k(t) - \hat{x}_k(t)$, we can write (44) as

$$\begin{bmatrix} e_k(t) \\ \hat{x}_k(t) \end{bmatrix} = \underbrace{\begin{bmatrix} I & 0 \\ -I & I \end{bmatrix}}_{\tilde{T}} \begin{bmatrix} e_k(t) \\ x_k(t) \end{bmatrix}. \quad (48)$$

By utilizing (48), the system (44) can be written as

$$\begin{bmatrix} \dot{e}_k(t) \\ \dot{\hat{x}}_k(t) \end{bmatrix} = \tilde{A}_a(\rho_k) \begin{bmatrix} e_k(t) \\ \hat{x}_k(t) \end{bmatrix} + \tilde{B}_a(\rho_k)\Lambda(t)\tilde{C}_a(\rho_k) \begin{bmatrix} e_k(t) \\ \hat{x}_k(t) \end{bmatrix}, \quad (49)$$

where

$$\tilde{A}_a(\rho_k) = \begin{bmatrix} M(\rho_k) & 0 \\ A_c(\rho_k) - M(\rho_k) & A_c(\rho_k) - B_v F(\rho_k) \end{bmatrix},$$

$$\tilde{B}_a(\rho_k) = \begin{bmatrix} -\dot{H}(\rho_k)C_k + (I - H(\rho_k)C_k)D_k(\rho_k)\tilde{\psi}_k & 0 & 0 \\ \dot{H}(\rho_k)C_k + (I - H(\rho_k)C_k)D_k(\rho_k)\tilde{\psi}_k & \tilde{B} & \tilde{B} \end{bmatrix},$$

$$\tilde{C}_a(\rho_k) = \begin{bmatrix} I & I \\ G_k C_k A_k(\rho_k) & G_k C_k A_k(\rho_k) + F(\rho_k) \\ I & I \end{bmatrix}.$$

To assure the boundedness on the uncertain term $\tilde{\Phi}(t)$ in (47), it is sufficient to ensure that the pseudo-inverse of $B_2 E_k(\rho_k)$ is norm bounded. By utilizing the property of pseudo-inverse, it is straightforward to show that for all combinations of $0 < \hat{w}_m(t) \leq 1$,

$$\begin{aligned} \left\| \tilde{\Phi}(t) \right\| &\leq \left\| B_1 B_2^T \right\| + \|B_1\| \, \|E_k(\rho_k)\| \, (1 + \Delta_{max}) \\ &\quad \times \|E_k(\rho_k))\ddagger\| \left\| (I - B_2\psi(t, \rho))^{-1} \right\| \\ &\leq \gamma_1 (1 + \frac{c(1 + \Delta_{max})}{1 - \frac{\Delta_{max} c}{\sqrt{\epsilon}}}), \end{aligned} \quad (50)$$

where $\gamma_1 = \|B_1\|$ and $\|B_2\|^T = 1$. The augmented uncertainty term in (47) is assumed to be norm-bounded and is defined as

$$\|\Lambda(t)\| < \gamma_\delta. \quad (51)$$

In nominal scenarios (i.e $\Delta_k(t) = 0$ and $\widehat{W}_k(t) = I$), the augmented closed loop system in (49) becomes

$$\begin{bmatrix} \dot{e}_k(t) \\ \dot{\hat{x}}_k(t) \end{bmatrix} = \tilde{A}_a(\rho_k) \begin{bmatrix} e_k(t) \\ \hat{x}_k(t) \end{bmatrix}, \quad (52)$$

where the stability of matrix $\tilde{A}_a(\rho_k)$ depends on the diagonal entries $M(\rho_k)$ and $A_c(\rho_k) - B_v F(\rho_k)$ which are made stable individually by selecting the appropriate observer gain $L_1(\rho_k)$ and controller gain $F(\rho_k)$. As a result, the overall system is stable. However, it is critical to ensure the stability of the closed-loop system in the event of actuator failures/faults. To do so, define a scalar $\gamma_2 > 0$ as a $\mathcal{L}_2$ norm linked with the term $\tilde{G}_{\mathcal{L}}(s)$ i.e.

$$\gamma_2 = \|\tilde{G}_{\mathcal{L}}(s)\|, \quad (53)$$

where $\tilde{G}_{\mathcal{L}}(s) = \tilde{C}_a(\rho_k)(sI - \tilde{A}_a(\rho_k))^{-1}\tilde{B}_a(\rho_k)$.

Proposition 1: The closed loop system in (49) is stable for any combination of actuator failures or faults belonging to the set $W_k(t) \in W_\delta$ and for all $\rho_k \in \Omega$.

$$\gamma_2 \gamma_\delta < 1. \quad (54)$$

Proof: In order to satisfy the CLS condition in (54), the augmented system defined in (49) is expressed as

$$\begin{bmatrix} \dot{e}_k(t) \\ \dot{\hat{x}}_k(t) \end{bmatrix} = \tilde{A}_a(\rho_k) \begin{bmatrix} e_k(t) \\ \hat{x}_k(t) \end{bmatrix} + \tilde{B}_a(\rho_k)\tilde{u}_a(t) \quad (55)$$

$$\tilde{y}_a(t) = \tilde{C}_a(\rho_k) \begin{bmatrix} e_k(t) \\ \hat{x}_k(t) \end{bmatrix}, \quad (56)$$

where

$$\tilde{u}_a(t) = \Lambda(t)\tilde{y}_a(t). \quad (57)$$

By writing augmented system (49) into the form (55), it may be regarded as feedback connection of linear term $\tilde{G}_{\mathcal{L}}(s)$ (53) and bounded uncertain term $\Lambda(t)$. Then, by employing a small gain theorem [38], if the stability condition (54) is satisfied then closed loop uncertain system (49) is stable. This complete the proof.

B. LPV INTEGRAL SLIDING MODE CONTROLLER

An LPV ISMC can be designed in the form as

$$v_k(t) = (G_k C_k B_w(\rho_k))^{-1}(v_l(t) + v_n(t)), \quad (58)$$

where

$$v_l(t) = -F(\rho_k)\hat{x}_k(t) - G_k C_k A_k(\rho_k)\hat{x}_k(t), \quad (59)$$

and the nonlinear term $v_n(t)$ is

$$v_n(t) = -k_\delta(t)\frac{\sigma_k(t)}{\|\sigma_k(t)\|}, \quad (60)$$

where $k_\delta(t)$ denotes the modulation gain, whose precise value is discussed in the next section.

Proposition 2: The designed nonlinear ISMC control law in (58) imposes the sliding motion into the sliding manifold for all allowable sets of failures or faults associated with the set W_ϵ and for all $\rho_k \in \Omega$ provided the k_δ is chosen as

$$\begin{aligned} k_\delta(t) \geq \|G_k\| \, \|C_k\| \, \|A_k(\rho_k)\| \, \|e_k\| + \|G_k\| \, \|C_k\| \\ \times \|D_k(\rho_k)\| \, \|\psi_k(t, x_k)\| \, \|x_k(t)\| + \eta_\delta, \end{aligned} \quad (61)$$

where $\eta_\delta > 0$.

Proof: To check the control law in (58) satisfies the reachability condition for the sliding surface, substitute (58) into (21) and further simplification yields

$$\dot{\sigma}_k(t) = G_k C_k A_k(\rho_k) x_k(t) + v_l(t) + v_n(t) + F(\rho_k)\hat{x}_k(t) + G_k C_k D_k(\rho_k) d_k(t, x_k). \tag{62}$$

Substitute the values of $v_l(t)$ and $v_n(t)$ from (58-(60) respectively and by taking considering the fact that $e_k(t) = x_k(t) - \hat{x}_k(t)$, the switching function in (62) is expressed as

$$\dot{\sigma_k}(t) = G_k C_k A_k(\rho_k) e_k(t) - k_\delta(t)\frac{\sigma_k(t)}{\|\sigma_k(t)\|} + G_k C_k D_k(\rho_k) d_k(t, x_k). \tag{63}$$

Multiply the left and right hand side of (63) with ${\sigma_k}^T(t)$, results

$$\begin{aligned}{\sigma_k}^T(t)\dot{\sigma}_k(t) &= {\sigma_k}^T(t) G_k C_k A_k(\rho_k) e_k(t) - k_\delta(t)\,\|\sigma_k(t)\| \\ &\quad + \|G_k C_k D_k(\rho_k) d_k(t, x_k)\| \\ &\le \|\sigma_k\|\,\|G_k C_k A_k(\rho_k) e_k(t)\| - k_\delta(t)\,\|\sigma_k(t)\| \\ &\quad + \|G_k C_k D_k(\rho_k) d_k(t, x_k)\| \\ &\le -\|\sigma_k\|\,(k_\delta(t) - \|G_k\|\,\|C_k\|\,\|A_k(\rho_k)\|\,\|e_k(t)\|) \\ &\quad + \|G_k\|\,\|C_k\|\,\|D_k(\rho_k)\|\,\|\psi_k(t, x_k)\|\,\|x_k(t)\|.\end{aligned} \tag{64}$$

Next after substituting the modulation gain k_δ defined in (61) into (64) and the derivative of Lyapunov function with respect to time ${\sigma_k}^T(t)\dot{\sigma}_k(t)$ along the system trajectory after simplifying becomes

$${\sigma_k}^T(t)\dot{\sigma}_k(t) \le -\eta_\delta\,\|\sigma_k(t)\|\,. \tag{65}$$

Hence so-called reachability condition is satisfied for all the time which can be verified from condition (65).
Finally, using (58),(59) and (60), the actual control input (9) is finally obtained as

$$u_k(t) = \widehat{W}_k(t)(E_k(\rho_k))^{-1} B_2^T (B_2 E_k(\rho_k)\widehat{W}_k(t)(E_k(\rho_k))^{-1} B_2^T)^{-1}\big(-F(\rho_k) - G_k C_k A_k(\rho_k))\hat{x}_k(t) - k_\delta(t)\frac{\sigma_k(t)}{\|\sigma_k(t)\|}\big). \tag{66}$$

Algorithm for Proposed FTC Scheme: In this section, a step-wise procedure is provided to demonstrate the implementation of the proposed scheme.

- The input distribution matrix $B_k(\rho_k)$ is first partitioned into fixed B_f and parameter-dependent matrix $E_k(\rho_k)$ according to (3).
- The fixed matrix B_f is further partitioned to the form (4) to resolve actuator redundancy. This may be achieved by appropriate state reordering and scaling is performed to further ensure $B_2 B_2^T = I_l$.
- Consider the pair (A_k, B_v) is controllable, design a state feedback gain $F(\rho_k)$ to make nominal closed-loop system (17) quadratically stable. The LMI procedure to obtain $F(\rho_k)$ is given in [34].

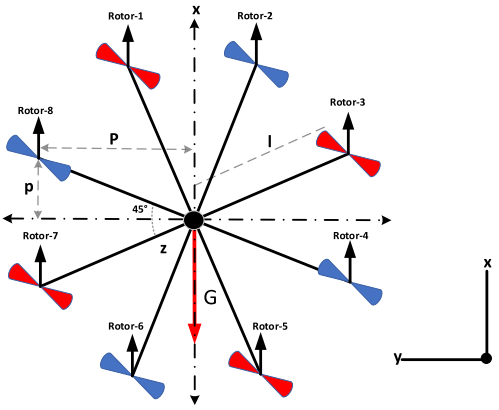

FIGURE 2. Star shaped octarotor.

- Design an LPV-UIO to estimate unknown states using observer dynamics in (34) and observer gain $L(\rho_k)$ is designed using MATLAB synthesis code "msfsyn".
- Design a virtual control law using (58-60) where $\sigma_k(t)$ is defined in (18).
- Finally the physical control law $u_k(t)$ is obtained using the (9).
- With the selection of controller gain $F(\rho_k)$ and observer gain $L(\rho_k)$, calculate the $\mathcal{L}_2$ norm γ_2. If $\gamma_2 \le 1/\gamma_\delta$, then the stability requirement in (54) is met, otherwise consider redesigning of $F(\rho_k)$ and $L(\rho_k)$.

V. MODELING OF OCTAROTOR

The effectiveness of the aforementioned strategy is assessed on the LPV model of an octarotor UAV system and afterward verified on a 6-DoF nonlinear model. The star-shaped octarotor is comprised of eight rods that are interconnected by a central plate, which houses the power supply and avionics systems of the vehicle. Each arm is positioned at a 45Â° angle, as depicted in Fig. 2. The dynamics equations of octarotor are described as [39].

$$\begin{cases} \ddot{x}_e = (cos\phi_e sin\theta_e cos\psi_e + sin\phi_e sin\psi_e)\dfrac{1}{m}U_4 \\ \ddot{y}_e = (cos\phi_e sin\theta_e sin\psi_e - sin\phi_e cos\psi_e)\dfrac{1}{m}U_4 \\ \ddot{z}_e = -g + a_1 b_z U_4 \\ \dot{p}_e = a_2 q_e r_e - a_3 q_e \omega + a_4 U_1 \\ \dot{q}_e = a_5 p_e r_e - a_6 p\omega + a_7 U_2 \\ \dot{r}_e = a_8 p_e q_e - a_9 U_3, \end{cases} \tag{67}$$

where x_e, y_e and z_e are the output of the system, which depicts the position of the vehicle, θ_e, ϕ_e and ψ_e denote the pitch, roll, and yaw angles, while p_e, q_e and r_e denotes angular velocity. All x_e, y_e, z_e, p_e, q_e and r_e are described with respect to the body fixed frame. The constant parameters are given by

$$\begin{cases} a_1 = \dfrac{1}{m}, a_2 = \dfrac{I_y - I_z}{I_x}, a_3 = \dfrac{J_r}{I_x}, a_4 = \dfrac{1}{I_x} \\ a_5 = \dfrac{I_z - I_x}{I_y}, a_6 = \dfrac{J_r}{I_y}, a_7 = \dfrac{1}{I_y} \\ a_8 = \dfrac{I_x - I_y}{I_z}, a_9 = \dfrac{1}{I_z}, b_z = cos\phi sin\theta. \end{cases} \tag{68}$$

To obtain the same entities in the earth fixed frame, the transformation matrix used is given as.

$$\begin{bmatrix} \dot{\phi}_e \\ \dot{\theta}_e \\ \dot{\psi}_e \end{bmatrix} = \begin{bmatrix} 1 & sin\phi_e tan\theta_e & cos\phi_e tan\theta_e \\ 0 & cos\phi_e & -sin\phi_e \\ 0 & \frac{sin\phi_e}{cos\theta_e} & \frac{cos\phi_e}{cos\theta_e} \end{bmatrix} \begin{bmatrix} p_e \\ q_e \\ r_e \end{bmatrix}. \tag{69}$$

The plant inputs $U_1(t), \ldots U_4(t))$ can be expressed as individual contributions from each of the eight rotors as

$$u_\tau(t) = B_\Omega u_k(t), \tag{70}$$

where $u_\tau(t) = [U_1, U_2, U_3, U_4]$ and $u_k(t)$ is defined as

$$u_k(t) = \begin{bmatrix} \Omega_1(t)^2 & \Omega_2(t)^2 \ldots & \Omega_8(t) \end{bmatrix}^T, \tag{71}$$

where $\Omega_i, i = 1 \ldots .8$ represents the speed of rotor. The fixed matrix B_Ω is defined as

$$B_\Omega = \begin{bmatrix} b & b & b & b & b & b & b & b \\ 0 & 0 & -bl & -bl & 0 & 0 & bl & bl \\ bl & bl & 0 & 0 & -bl & -bl & 0 & 0 \\ -d & -d & d & d & -d & -d & d & d \end{bmatrix}, \tag{72}$$

where l is the moment arm length (for octarotor $l = Lcos\frac{\pi}{8}$ and L is the arm length). The fixed scalars b and d in (72) denotes the thrust and drag factor respectively.

LPV Model of UAV: Similar to existing work, a two-loop control structure is proposed to attain 6-DoF motion control of UAV. Therefore the states associated with inner loop dynamics, which are directly related to control inputs, are converted into LPV form. The inner-loop state vector is defined as

$$x_k = \begin{bmatrix} z_e & \phi_e & \theta_e & \psi_e & \dot{z}_e & p_e & q_e & r_e \end{bmatrix}^T. \tag{73}$$

It should be noted that the states x_e and y_e, as well as their derivative $\dot{x}_e$ and $\dot{y}_e$, are not encompassed in (73) for the purpose of designing the inner loop (rate) controller. This phenomenon arises from the conventional practice of utilizing the pitch and roll angles as manipulated variables to regulate the x_e and y_e coordinates of the octarotor [39]. To further assist the controller synthesis, it is assumed that the perturbations from hover flights are smaller than the following approximation $(\dot{\phi}_e, \dot{\theta}_e, \dot{\psi}_e) = (p_e, q_e, r_e)$ holds. Therefore, the nonlinear system (67) associated with state vector (73) is written into LPV form (1) by considering the following set of scheduling variable ρ_k defined as

$$\begin{aligned} \rho_k &= \begin{bmatrix} \rho_{k_1} & \rho_{k_2} & \rho_{k_3} & \rho_{k_4} \end{bmatrix} \\ &= \begin{bmatrix} p_e(t) & q_e(t) & r_e(t) & b_z \end{bmatrix}, \end{aligned} \tag{74}$$

The parameter-dependent matrices LPV system are defined as

$$\begin{aligned} A_k(\rho_k) &= \begin{bmatrix} 0_{4\times4} & I_{4\times4} \\ 0_{4\times4} & A_{22}(\rho_k) \end{bmatrix}, \quad B_k(\rho_k) = \begin{bmatrix} 0_{4\times4} \\ B_{21}(\rho_k) \end{bmatrix}, \\ C_k &= \begin{bmatrix} I_4 & 0_4 \end{bmatrix}, D_k(\rho_k) = \begin{bmatrix} 0_{4\times4} \\ D_{21}(\rho_k) \end{bmatrix}, \end{aligned} \tag{75}$$

where

$$A_{22} = \begin{bmatrix} 0 & 0 & 0 & 0 \\ 0 & 0 & \frac{a_2}{2}\rho_{k_3} & \frac{a_2}{2}\rho_{k_2} \\ 0 & \frac{a_5}{2}\rho_{k_3} & 0 & \frac{a_5}{2}\rho_{k_1} \\ 0 & \frac{a_8}{2}\rho_{k_2} & \frac{a_8}{2}\rho_{k_1} & 0 \end{bmatrix},$$

$$B_{21}(\rho_k) = \begin{bmatrix} -\rho_{k_4}a_1 & 0 & 0 & 0 \\ 0 & a_4 & 0 & 0 \\ 0 & 0 & a_7 & 0 \\ 0 & 0 & 0 & a_9 \end{bmatrix}, \text{ and}$$

$$D_{21}(\rho_k) = \begin{bmatrix} 0 & 1 \\ a_3\rho_{k_2} & 0 \\ -a_6\rho_{k_1} & 0 \\ 0 & 0 \end{bmatrix}.$$

Using torque/force-rotor speed mapping given in (71-72), the LPV system (1) can also be represented as

$$\dot{x}_k(t) = A_k(\rho_k)x_k(t) + B_k(\rho_k)(1_8 - \Delta_k(t))\widehat{W}_k(t)u_k(t), \tag{76}$$

where $B_k(\rho_k) = B_\tau(\rho_k)B_\Omega$. Based on the structure of B_τ and B_Ω, $B_k(\rho_k)$ can be perfectly factorized into fixed and varying component (3)

$$B_k(\rho_k) = B_f E_k(\rho_k), \tag{77}$$

where $B_f = \begin{bmatrix} 0_4 \times 4 \\ I_4 \end{bmatrix}$ and $E_k(\rho_k)$ is defined in (78), as shown at the bottom of the next page, where b symbolizes the lift coefficient, l denotes the distance from center of each rotor to the center of gravity, d designates the force-to-moment scaling factor.

VI. CONTROLLER PARAMETERS SETTINGS AND NUMERICAL SIMULATIONS

A. CONTROLLER PARAMETERS SETTINGS

The parameters of nonlinear model are $m = 1.3Kg, g = 9.8\ m/s^2, I_x, I_y = 0.0150, I_z = 0.0026, j_r = 6 \times 10^{-5}, b = 3.13 \times 10^{-5}$, and $d = 7.5 \times 10^{-7}$ [39]. Note that B_f is already in the form given in (4) and it can be verified that $B_2B_2^T = I_4$, $\|B_2\| > \|B_1\|$ and $\|B_2\| = 1$. The controller gain is computed by using a fixed Lyapunov function that results in designing of gain $F(\rho_k)$ by using Matlab LMI multi-model state-feedback synthesis code "msfsyn" to solve the LMIs. LQR type cost function was selected. It is a trade-off between performance and actuator effort. The parameters Q_k and R_k are adjusted to meet the desired performance by considering energy constraints. The matrices Q_k and R_k are taken as $Q_k = diag[1, 0.001, 1, 0.001, 1, 0.001, 1, 0.001]$ and $R_k = diag[2.4, 2.4, 2.4, 2.4]$. The feedback gain matrix F value comes out as shown in the equation at the bottom of the next page, Over the entire working regime, a fixed observer gain $L(\rho_k) = L$ is acceptable and is implemented with the "msfsyn" command in the MATLAB, where, LMIs are solved for observer gain using the duality property, i.e.

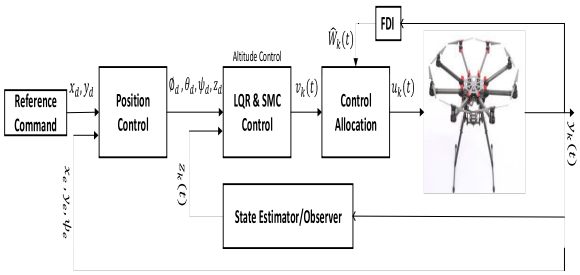

FIGURE 3. Architecture of controller implementation to octarotor system.

observability of $(T(\rho_k)A_k(\rho_k), C_k)$ implies controllability of $\left((T(\rho_k)A_k(\rho_k))^T, C_k^T\right)$. The observer gain L_1 is computed as

$$L = \begin{bmatrix} 8.6 & 0 & 0 & 0 & 17.85 & 0 & 0 & 0 \\ 0 & 6.6 & 0 & 0 & 0 & 10.85 & 0 & 0 \\ 0 & 0 & 7.8 & 0 & 0 & 0 & 14.85 & 0 \\ 0 & 0 & 0 & 6.3 & 0 & 0 & 0 & 9.9 \end{bmatrix}.$$

With the choice of $F(\rho_k)$, the scalar γ_2 is computed as 0.24. Therefore, the norm on uncertainty should satisfy $\gamma_\delta < 1/0.24$ to satisfy the closed-loop stability. The sliding gain $k_\delta(t)$ is selected as 5.928 to satisfy the reachability condition and $\eta_\delta = 0.005$. In order to track the desired position in both the x and y directions, a PID structure in the outer loop subsystem has been taken into account.

$$\begin{cases} \ddot{x}_c = \ddot{x}_d + k_{d_x}(\dot{x}_d - \dot{x}_e) + k_{p_x}(x_d - x_e) \\ \ddot{x}_c = \ddot{y}_d + k_{d_y}(\dot{y}_d - \dot{y}_e) + k_{p_y}(y_d - y_e), \end{cases} \tag{79}$$

where the position controller gains are chosen as $k_{d_x} = 5.6$, $k_{p_x} = 0.9$, $k_{d_y} = 0.2$, $k_{p_y} = 0.2$. In order to compute the desired roll and pitch commands for the inner loop subsystem,

$$\begin{cases} \phi_d = (\ddot{x}_c sin(\psi_{des}) - \ddot{y}_c cos(\psi_{des}))/g \\ \theta_d = (\ddot{x}_c cos(\psi_{des}) - \ddot{y}_c sin(\psi_{des}))/g. \end{cases} \tag{80}$$

Figure 3 illustrates the comprehensive arrangement of the outer loop PID control and inner loop ISMC with CA scheme. The resulting signals from the PID controller are utilized as the command signal for roll and pitch angles to the inner loop subsystem. In the interest of simplicity, the command signal for yaw angle is deliberately set to zero.

B. ACTUATOR FAULT RECONSTRUCTION SCHEME

In the LPV observer design section, it is mentioned that the fault term $\hat{K}u(t)$ is decoupled from the error dynamics using the suitable choice of $M(\rho_k)$ and $H(\rho_k)$ matrices. The fault term $\hat{K}u(t)$ can be reconstructed using the concept given in [34],specifically

$$\hat{K}u(t) \approx ((B_f E_k(\rho_k))^T B_f E(\rho_k))^{-1}(B_f E_k(\rho_k))^T \upsilon_\delta(t) \tag{81}$$

where $\upsilon_\delta(t)$ is the injection term necessary to maintain sliding. The injection term is discontinuous and can be approximated to any level of accuracy. The scalar $\hat{k}_i(t)$ can be obtained by introducing a small threshold ε such that if at time t_ε, $\mid u_i(t) \mid \leq \varepsilon$, then

$$\hat{k}_i(t) = \begin{cases} \dfrac{((B_f E_k(\rho_k))^T B_f E_k(\rho_k))^{-1}(B_f E_k(\rho_k))^T \upsilon_\delta(t)}{u_i(t)} \\ \qquad if\,|u_i(t)| > \varepsilon \\ \hat{k}_i(t_\epsilon) \quad otherwise \end{cases} \tag{82}$$

where

$$\upsilon_\delta(t) := -\rho_e \frac{e_k(t)}{\|e_k(t)\| + \delta} \tag{83}$$

where δ is a small positive scalar, $e_k(t)$ is defined in (38) and the scalar ρ_e must be chosen such that $\rho_e \geq \left\|\hat{K}(t)u(t)\right\|$.

VII. SIMULATIONS AND RESULTS

The simulations in this section are performed with the primary aim of demonstrating the effectiveness of the proposed methodology. The simulations contain a wide range of combinations that involve faults/failures in the actuator channel including the imperfection in the estimation. The following analysis applies to the performance of closed-loop tracking. The proposed methodology is executed and simulated using the MATLAB/Simulink platform. The evaluation process entails the exploration of three distinct scenarios

- In the initial scenario, the performance of the octarotor is evaluated under nominal settings, where it is assigned the responsibility of accurately following a predetermined reference trajectory.
- Subsequently, the trajectory tracking is evaluated with partial faults/failure in rotors.

$$E_k(\rho_k) = \begin{bmatrix} -\rho_{k_4} a_1 b & -\rho_{k_4} a_1 b & -\rho_{k_4} a_1 b & -\rho_{k_4} a_1 b & -\rho_{k_4} a_1 b & -\rho_{k_4} a_1 b & -\rho_{k_4} a_1 b & -\rho_{k_4} a_1 b \\ 0 & 0 & -a_4 bl & -a_4 bl & 0 & 0 & a_4 bl & a_4 bl \\ a_7 bl & a_7 bl & 0 & 0 & -a_7 bl & -a_7 bl & 0 & 0 \\ -a_9 d & -a_9 d & a_9 d & a_9 d & -a_9 d & -a_9 d & a_9 d & a_9 d \end{bmatrix}, \tag{78}$$

$$F = \begin{bmatrix} 0.43 & -0.12 & 0.21 & 0.40 & 8.03 & -0.31 & -0.93 & 0.10 \\ -0.48 & -0.11 & 0.19 & 0.36 & -0.31 & 8.10 & -0.84 & 0.09 \\ 0.00 & 0.01 & 0.57 & -0.29 & -0.72 & -0.64 & 6.41 & -0.54 \\ 0.00 & -0.62 & -0.07 & -0.28 & -0.10 & -0.09 & -0.27 & 1.82 \end{bmatrix}.$$

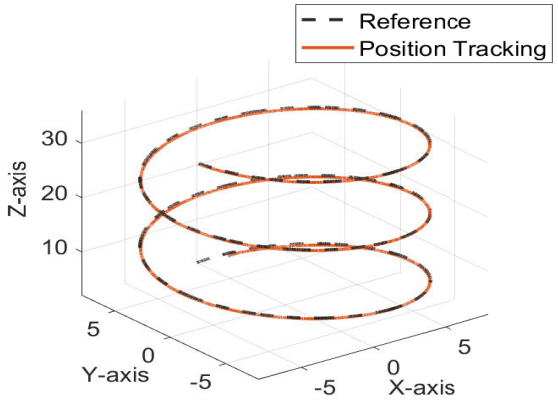

FIGURE 4. 3D View of desired trajectory tracking under nominal conditions.

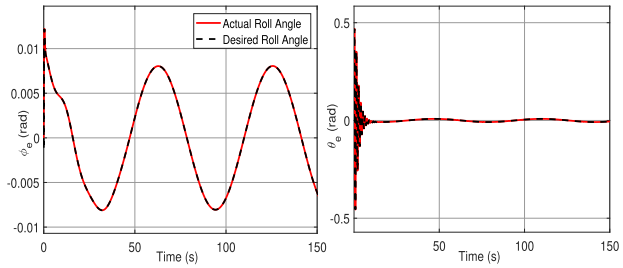

FIGURE 5. Octarotor roll and pitch angle tracking at nominal condition.

- In the third case performance is assessed under the worst-case scenario, which involves the failure of all the redundant rotors during the flight state.

Throughout the simulations, it is assumed that no two rotors in a pair (1, 2), (3, 4), (5, 6) and (7, 8) failed completely.

A. CASE 1: REFERENCE TRAJECTORY TRACKING UNDER NOMINAL CONDITION

In this study, the simulations are conducted to attain a reference trajectory with a focus on achieving the nominal performance. The desired tracking signals for $x - y$ position are sine and cosine signals of amplitude 8 m and frequency $1Hz$, while the desired altitude signal is a ramp signal with initial amplitude $2m$ and slew rate is 0.2 m/s and the desired yaw angle is set to zero. The simulation results depicted in Fig. 4 show a meticulous evaluation of the desired trajectory versus the actual measured trajectory. The attitude tracking results, presented in Figures 5 and 6, show an excellent performance of the proposed scheme in the nominal condition. This demonstrates that the designed LPV controller works well in the nominal condition. The plots of speed of individual rotors are given in Figures 7 and 8. It can be seen that all the rotors are contributing to achieving the flight path in nominal conditions.

B. CASE 2: REFERENCE TRAJECTORY TRACKING WITH ACTUATOR FAULTS AND FAILURES CONDITION

The simulation aims to examine the ability of an octarotor to accurately follow a predetermined trajectory in the presence

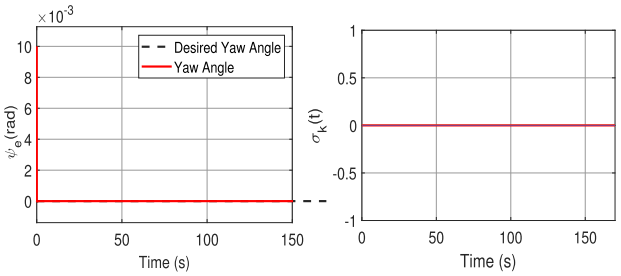

FIGURE 6. Octarotor Yaw angle tracking at nominal condition.

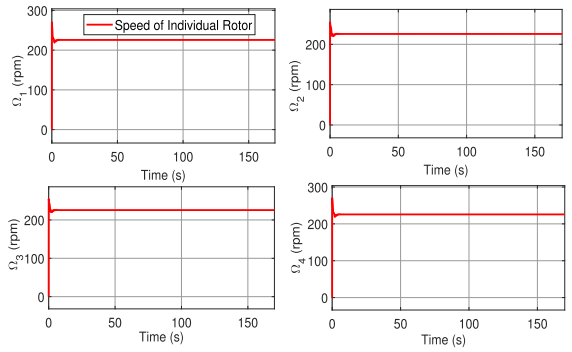

FIGURE 7. Speed of individual Rotors-1 to 4.

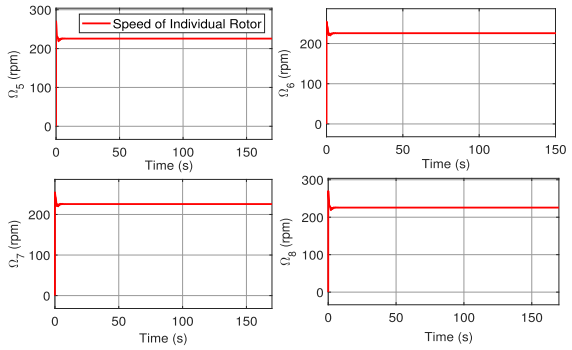

FIGURE 8. Speed of individual Rotors-5 to 8.

of malfunctioning of two or more actuators. It should be noted that the same desired reference trajectories are provided as in the nominal scenarios. To test the faults and failure conditions, the rotors 5 and 8 lost their effectiveness up to 50% after 25 s and 90 s, while, the rotors 2 and 3 were subjected to complete failure after 25 s and 90 s respectively. The failed rotors are not able to contribute towards desired reference tracking. However, all the remaining four rotors are assumed to be working perfectly. Remarkably, as shown in Figures. 9, 10 and 11, the octarotor successfully maintains its intended trajectory despite the disturbance and rotor failures. In the case of desired yaw angle tracking, a slight deviation becomes evident subsequent to the malfunctioning of rotors 2 and 3. However, it is noteworthy that the deviation is kept within the tolerable limit and the yaw angle state remains close to the predetermined nominal path. The plots of the speed of individual rotors are given in Figure 12 and 13. It is notable that rotors 1, 4, 6, and 7 increase their control effort to maintain tracking and desired performance while the speed of rotors 2 and 3 reduced to zero after $25s$ and $90s$ respectively.

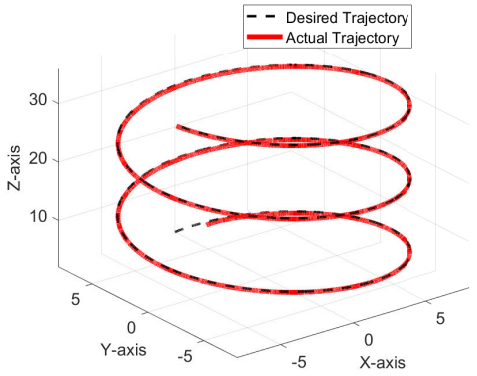

FIGURE 9. 3D view of desired trajectory tracking in case of fault and failure.

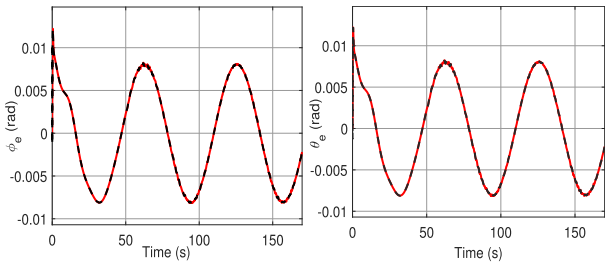

FIGURE 10. Roll and pitch angle tracking under fault/failure conditions.

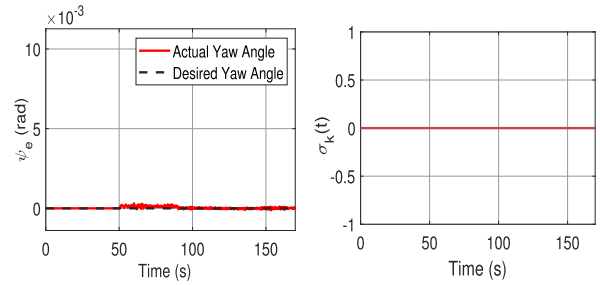

FIGURE 11. Yaw angle tracking under fault/failure condition.

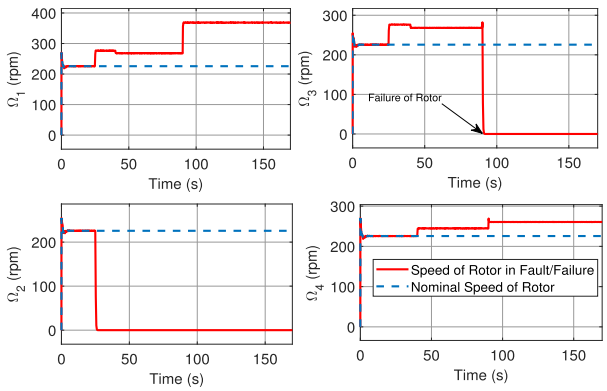

FIGURE 12. Speed of individual rotors; 1 to 4.

This illustrates the effectiveness of the CA scheme in terms of the redistribution of control signals among the available redundant actuators.

C. CASE 4: FAILURE WITH IMPERFECT ESTIMATION

In this simulation, different imperfection levels are introduced in the measurement of the actuator effectiveness level.

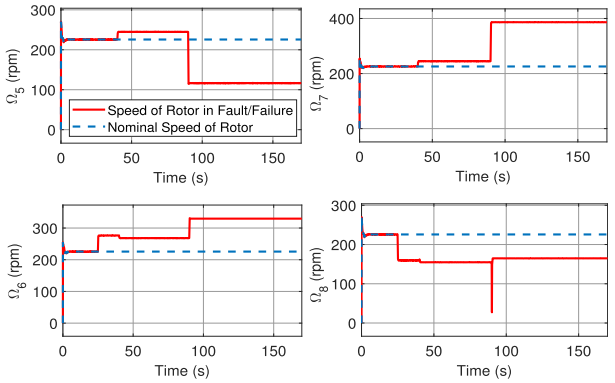

FIGURE 13. Speed of individual rotors; 5 to 8.

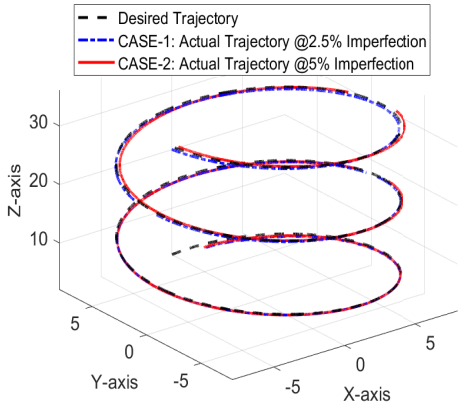

FIGURE 14. 3D view of desired trajectory tracking with imperfect estimation.

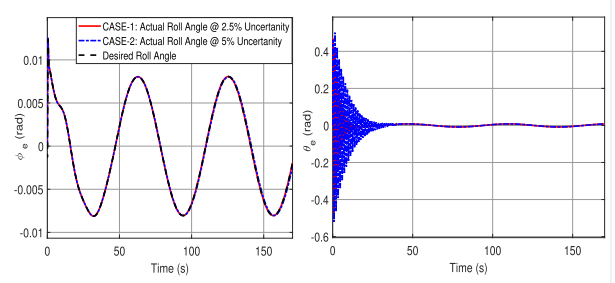

FIGURE 15. Roll and pitch angle tracking subject to imperfect estimation.

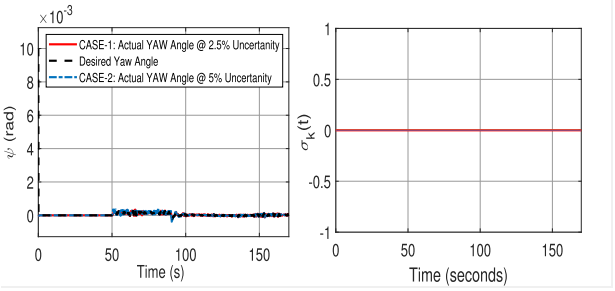

FIGURE 16. Yaw angle tracking with imperfect estimation.

Theoretically, the maximum percentage error Δ_{max} that the proposed scheme can withstand and yet ensure the stability condition of proposition 1 is 5.5%. However, to simulate the theoretical findings, two different levels of imperfectness are

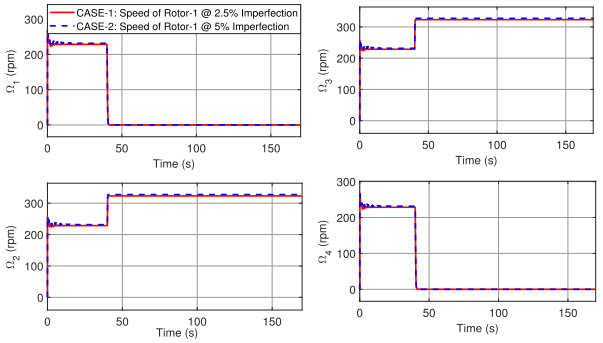

FIGURE 17. Speed of individual rotors with imperfect estimation: Rotor 1 to 4.

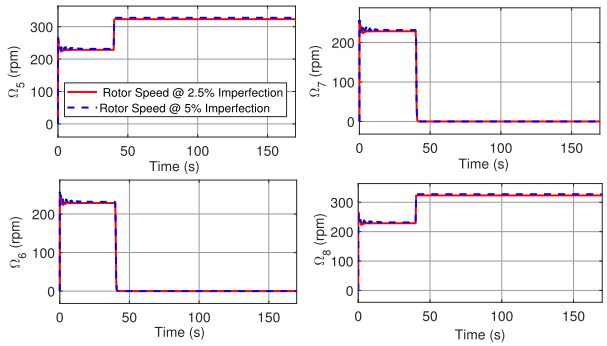

FIGURE 18. Speed of individual rotors with imperfect estimation: Rotor 5 to 8.

considered to analyze the closed-loop stability and tracking performance. The desired reference trajectory in this case is similar to the first two cases. To test the fault-tolerant condition, the failure condition is introduced to rotors 1, 4, 6, and 7 after 40 s. Two imperfection levels are introduced in the estimate of rotor effectiveness level i.e. 2% and 5%. The simulation plots showing the tracking performance are provided in Figures 14, 15, and 16. The tracking response clearly shows that the system states are following the desired trajectories nominally. However, a slight deviation can be observed in the case of pitch and yaw angle tracking. The control redistribution curves in Figures 17 and 18 show the redistribution of control effort among the healthy redundant rotors 2, 3, 5, and 8 in case of failure of the associated rotors. This shows the dominant performance of the proposed CA scheme. The plot of the switching function in Figure 18 shows that sliding motion is maintained all the time.

D. CONCLUSION

This work proposed a nonlinear ISM fault-tolerant CA scheme for the class of LPV system in an output feedback frame. The CA unit relies on the information of actuator healthiness level to redistribute the control signals among the available redundant actuators. In this work, imperfect estimation information is included in the controller synthesis procedure and closed-loop stability conditions are derived to ensure the system stability up to a certain extent of fault estimation error. The numerical simulations are carried out on a 6-degree-of-freedom nonlinear model of octarotor UAV system expressed in LPV form. Various fault and failure conditions including imperfect estimations, are included in the simulation to demonstrate the effectiveness of the proposed method. In future work, a sensor fault estimation scheme will be considered and an adaptive adjustable dimension observer, similar to the one proposed in [40], will be designed for the class of LPV system.

REFERENCES

[1] Y. Liu, S. Hong, E. Zio, and J. Liu, "Integrated fault estimation and fault-tolerant control for a flexible regional aircraft," *Chin. J. Aeronaut.*, vol. 35, no. 3, pp. 390–399, Mar. 2022, doi: 10.1016/j.cja.2021.05.025.

[2] Y. Zhu and W. X. Zheng, "An integrated design approach for fault-tolerant control of switched LPV systems with actuator faults," *IEEE Trans. Syst., Man, Cybern., Syst.*, vol. 53, no. 2, pp. 908–921, Feb. 2023, doi: 10.1109/TSMC.2022.3189538.

[3] M. Zhu, X. Wang, Z. Dan, S. Zhang, and X. Pei, "Two freedom linear parameter varying μ synthesis control for flight environment testbed," *Chin. J. Aeronaut.*, vol. 32, no. 5, pp. 1204–1214, May 2019, doi: 10.1016/j.cja.2019.01.017.

[4] J. S. Shamma and M. Athans, "Guaranteed properties of gain scheduled control for linear parameter-varying plants," *Automatica*, vol. 27, no. 3, pp. 559–564, May 1991, doi: 10.1016/0005-1098(91)90116-j.

[5] D. Rotondo, V. Puig, and F. Nejjari, "A virtual actuator approach for fault tolerant control of switching LPV systems," *IFAC Proc. Volumes*, vol. 47, no. 3, pp. 11667–11672, 2014, doi: 10.3182/20140824-6-za-1003.00697.

[6] M. Rodrigues, H. Hamdi, N. BenHadj Braiek, and D. Theilliol, "Observer-based fault tolerant control design for a class of LPV descriptor systems," *J. Franklin Inst.*, vol. 351, no. 6, pp. 3104–3125, Jun. 2014, doi: 10.1016/j.jfranklin.2014.02.016.

[7] B. Rabaoui, H. Hamdi, N. B. Braiek, and M. Rodrigues, "A reconfigurable PID fault tolerant tracking controller design for LPV systems," *ISA Trans.*, vol. 98, pp. 173–185, Mar. 2020, doi: 10.1016/j.isatra.2019.08.049.

[8] D. Qiao and Y. Wang, "Fault-tolerant control for linear parameter varying systems with integral measurements based on event-triggered mechanism," *J. Franklin Inst.*, vol. 358, no. 16, pp. 8250–8269, Oct. 2021, doi: 10.1016/j.jfranklin.2021.08.018.

[9] G. Zong, D. Yang, J. Lam, and X. Song, "Fault-tolerant control of switched LPV systems: A bumpless transfer approach," *IEEE/ASME Trans. Mechatronics*, vol. 27, no. 3, pp. 1436–1446, Jun. 2022, doi: 10.1109/TMECH.2021.3096375.

[10] H. Peng, L. Wei, X. Zhu, W. Xu, and S. Zhang, "Aggressive maneuver oriented integrated fault-tolerant control of a 3-DOF helicopter with experimental validation," *Aerosp. Sci. Technol.*, vol. 120, Jan. 2022, Art. no. 107265.

[11] R. Tayari, A. Ben Brahim, F. Ben Hmida, and A. Sallami, "Active fault tolerant control design for LPV systems with simultaneous actuator and sensor faults," *Math. Problems Eng.*, vol. 2019, pp. 1–14, Jan. 2019, doi: 10.1155/2019/5820394.

[12] S. Ijaz, L. Yan, M. T. Hamayun, W. M. Baig, and C. Shi, "An adaptive LPV integral sliding mode FTC of dissimilar redundant actuation system for civil aircraft," *IEEE Access*, vol. 6, pp. 65960–65973, 2018, doi: 10.1109/ACCESS.2018.2876032.

[13] K. Han, J. Feng, and Q. Zhao, "Robust estimator-based dual-mode predictive fault-tolerant control for constrained linear parameter varying systems," *IEEE Trans. Ind. Informat.*, vol. 17, no. 7, pp. 4469–4479, Jul. 2021, doi: 10.1109/TII.2020.3022387.

[14] J. Han, X. Liu, X. Wei, and S. Sun, "A dynamic proportional-integral observer-based nonlinear fault-tolerant controller design for nonlinear system with partially unknown dynamic," *IEEE Trans. Syst., Man, Cybern., Syst.*, vol. 52, no. 8, pp. 5092–5104, Aug. 2022, doi: 10.1109/TSMC.2021.3114326.

[15] J. Han, X. Liu, X. Xie, and X. Wei, "Dynamic output feedback fault tolerant control for switched fuzzy systems with fast time varying and unbounded faults," *IEEE Trans. Fuzzy Syst.*, vol. 31, no. 9, pp. 3185–3196, Sep. 2023, doi: 10.1109/TFUZZ.2023.3246061.

[16] J. Han, X. Liu, X. Wei, and X. Zhu, "Reduced-order observer-based finite time fault estimation for switched systems with lager and fast time varying fault," *IEEE Trans. Circuits Syst. II, Exp. Briefs*, vol. 71, no. 1, pp. 350–354, Jan. 2024, doi: 10.1109/TCSII.2023.3304271.

[17] C. Wei, M. Wang, B. Lu, and J. Pu, "Accelerated Landweber iteration based control allocation for fault tolerant control of reusable launch vehicle," *Chin. J. Aeronaut.*, vol. 35, no. 2, pp. 175–184, Feb. 2022, doi: 10.1016/j.cja.2021.03.017.

[18] P. Vayalali, M. McKay, and F. Gandhi, "Redistributed pseudoinverse control allocation for actuator failure on a compound helicopter," in *Proc. Vertical Flight Soc. 76th Annu. Forum*, Oct. 2020, pp. 1–12.

[19] L. Kou, S. He, Y. Li, and J. Xiang, "Constrained control allocation of a quadrotor-like autonomous underwater vehicle," *J. Guid., Control, Dyn.*, vol. 44, no. 3, pp. 659–666, Mar. 2021.

[20] D.-F. Zhang, S.-P. Zhang, Z.-Q. Wang, and B.-C. Lu, "Dynamic control allocation algorithm for a class of distributed control systems," *Int. J. Control, Autom. Syst.*, vol. 18, no. 2, pp. 259–270, Feb. 2020.

[21] A. Argha, S. W. Su, and B. G. Celler, "Control allocation-based fault tolerant control," *Automatica*, vol. 103, pp. 408–417, May 2019.

[22] X. Yu and J. Jiang, "A survey of fault-tolerant controllers based on safety-related issues," *Annu. Rev. Control*, vol. 39, pp. 46–57, 2015.

[23] L. Chen, C. Edwards, H. Alwi, and M. Sato, "Flight evaluation of a sliding mode online control allocation scheme for fault tolerant control," *Automatica*, vol. 114, Apr. 2020, Art. no. 108829.

[24] J. C. Monteiro, F. Lizarralde, and L. Hsu, "Optimal control allocation of quadrotor UAVs subject to actuator constraints," in *Proc. Amer. Control Conf. (ACC)*, Jul. 2016, pp. 500–505.

[25] Y. Yan, J. Yang, C. Liu, M. Coombes, S. Li, and W.-H. Chen, "On the actuator dynamics of dynamic control allocation for a small fixed-wing UAV with direct lift control," *IEEE Trans. Control Syst. Technol.*, vol. 28, no. 3, pp. 984–991, May 2020.

[26] S. Ijaz, M. Galea, M. T. Hamayun, H. Ijaz, and U. Javaid, "A new output integral sliding mode fault-tolerant control and fault estimation scheme for uncertain systems," *IEEE Trans. Autom. Sci. Eng.*, 2023, doi: 10.1109/TASE.2023.3293318.

[27] B. Vanek, T. Péni, Z. Szabó, and J. Bokor, "Fault tolerant LPV control of the GTM UAV with dynamic control allocation," in *Proc. AIAA Guid., Navigat., Control Conf.*, 2014, p. 1148.

[28] K. Zhang, B. Jiang, X. Yan, and C. Edwards, "Interval sliding mode observer-based fault accommodation for non-minimum phase LPV systems with online control allocation," *Int. J. Control*, vol. 93, no. 11, pp. 2675–2689, Nov. 2020.

[29] M. T. Hamayun, S. Ijaz, and A. H. Bajodah, "Output integral sliding mode fault tolerant control scheme for LPV plants by incorporating control allocation," *IET Control Theory Appl.*, vol. 11, no. 12, pp. 1959–1967, Aug. 2017.

[30] L. Chen, H. Alwi, C. Edwards, and M. Sato, "Flight evaluation of an LPV sliding mode controller with online control allocation," in *Proc. IEEE 56th Annu. Conf. Decis. Control (CDC)*, Dec. 2017, pp. 3928–3933.

[31] I. Mizrak, H. Alwi, and C. Edwards, "Fault tolerant control of an octoplane UAV using sliding modes," in *Proc. 5th Int. Conf. Control Fault-Tolerant Syst. (SysTol)*, Sep. 2021, pp. 121–126.

[32] A. Argha, S. W. Su, A. Savkin, and B. G. Celler, "Novel frameworks for the design of fault-tolerant control using optimal sliding-mode control," *Int. J. Robust Nonlinear Control*, vol. 28, no. 8, pp. 3015–3032, May 2018.

[33] F. Cao, Z. Zhang, and X. He, "Active fault isolation of over-actuated systems based on a control allocation approach," *IEEE Trans. Instrum. Meas.*, vol. 71, pp. 1–10, 2022.

[34] M. T. Hamayun, C. Edwards, and H. Alwi, "Design and analysis of an integral sliding mode fault tolerant control scheme," in *Fault Tolerant Control Schemes Using Integral Sliding Mode*. Cham, Switzerland: Springer, 2016, pp. 39–61, doi: 10.1007/978-3-319-32238-4_3.

[35] M. T. Hamayun, C. Edwards, and H. Alwi, "A fault tolerant control allocation scheme with output integral sliding modes," *Automatica*, vol. 49, no. 6, pp. 1830–1837, Jun. 2013, doi: 10.1016/j.automatica.2013.02.043.

[36] M. T. Hamayun, C. Edwards, and H. Alwi, "Design and analysis of an integral sliding mode fault-tolerant control scheme," *IEEE Trans. Autom. Control*, vol. 57, no. 7, pp. 1783–1789, Jul. 2012.

[37] F. Castanos and L. Fridman, "Analysis and design of integral sliding manifolds for systems with unmatched perturbations," *IEEE Trans. Autom. Control*, vol. 51, no. 5, pp. 853–858, May 2006.

[38] S. Seshagiri and H. K. Khalil, "Robust output feedback regulation of minimum-phase nonlinear systems using conditional integrators," *Automatica*, vol. 41, no. 1, pp. 43–54, Jan. 2005.

[39] G. A. Victor and S. Adrian M. Stoica, "Integral LQR control of a star-shaped octorotor," *INCAS Bull.*, vol. 4, no. 2, pp. 3–18, Jun. 2012.

[40] J. Han, X. Liu, X. Wei, and X. Hu, "Adaptive adjustable dimension observer based fault estimation for switched fuzzy systems with unmeasurable premise variables," *Fuzzy Sets Syst.*, vol. 452, pp. 149–167, Jan. 2023, doi: 10.1016/j.fss.2022.06.017.

OMAR AZEEM received the bachelor's degree in electrical engineering from The University of Lahore, in 2012, and the master's degree in electrical engineering from the University of Central Punjab, Lahore, in 2017. He is currently pursuing the Ph.D. degree in electrical engineering with COMSATS University Islamabad, Lahore Campus. His research interests include integral sliding mode control, fault-tolerant control, and fault detection and isolation.

MIRZA TARIQ HAMAYUN is currently an Associate Professor with the Department of Electrical and Computer Engineering, COMSATS University Islamabad, Lahore Campus. He has been involved in the automation and control of high-speed power motors while working with the Daimler Chrysler AG Research Centre, Frankfurt, Germany. He has specifically worked on the development of so-called ISM controllers as a candidate for FTC. He is an author of more than 32 refereed papers, including one monograph for Springer-Verlag titled *Fault Tolerant Control Schemes Using Integral Sliding Modes*. His research interests include fault tolerant control, LPV control, sliding mode control, reconfigurable control, fault detection and isolation, and optimization control theory.

SALMAN IJAZ received the Ph.D. degree in control sciences and engineering from Beihang University (BUAA), Beijing, in 2018. From 2018 to 2020, he was a Postdoctoral Researcher with the Nanjing University of Aeronautics and Astronautics, Nanjing, China. He is currently an Assistant Professor with the School of Aerospace, University of Nottingham, Ningbo, China. He is also a member of the Key Laboratory of More Electric Aircraft of Zhejiang Province and a member of the Control Systems Laboratory. His current research interests include fault-tolerant control of aircraft systems, sliding mode control, control allocations, and UAV systems.

KHANSA TARIQ (Graduate Student Member, IEEE) received the master's degree in electrical engineering from COMSATS University Islamabad, Lahore Campus. She is currently pursuing the Ph.D. degree with the Department of Electrical Engineering, Lahore University of Management Sciences (LUMS), Lahore, Pakistan. Her research interests include analysis and control of socio-hydrological systems, model predictive control, and disaster risk assessment.